Received: 31 July 2024 | Revised: 2 December 2024 | Accepted: 22 December 2024

DOI: 10.1002/cac2.12651

CANCER COMMUNICATIONS Open Access

LETTER TO THE JOURNAL

Single-cell transcriptomics and epigenomics point to CD58-CD2 interaction in controlling primary melanoma growth and immunity

Immunotherapy is currently one of the most promising treatment options for malignant melanoma [1]. To uncover new immunological targets for future treatment approaches, single-cell transcriptomic and epigenomic analyses were performed on human primary melanoma (MM) and melanocytic nevus (Nev) samples (Figure 1A). The detailed methods of this study are described in the Supplementary Material.

MM and Nev biopsies (Supplementary Figure S1; Supplementary Table S1) were analyzed by single-cell RNA sequencing (scRNA-seq) and single-cell Assay for Transposase-Accessible Chromatin sequencing (scATAC-seq) (Supplementary Figure S2; Supplementary Tables S2 and S3). Using Uniform Manifold Approximation and Projection (UMAP), 28 distinct cellular clusters were identified and annotated based on scRNA-seq data from a previous report and manual curation (Figure 1B; Supplementary Figure S3A) [2]. Examples of gene expression patterns for individual cell types are provided in Supplementary Table S4. Lesional T lymphocytes were quantified using scRNA-seq data and anti-CD3 immunofluorescence staining, which revealed three distinct immune states: hot (>25 % T cells), intermediate (>6-25 % T cells), and cold (0-6 % T cells) (Supplementary Table S5).

Based on a previous study examining melanoma cell differentiation statuses, the melanoma cell cluster was divided into 8 distinct subclusters (Supplementary Figure S3B, C) [3]. Unsupervised clustering further refined these findings, predicting 11 cellular subclusters of melanoma cells (Figure 1C, Supplementary Table S6) [3].

To investigate the molecular mechanisms underlying melanoma cell dedifferentiation, RNA velocity and latent time (LT) analyses were performed (Supplementary Material and Methods). These analyses measure developmental processes based on the gene expression patterns of spliced and unspliced genes [4], with LT more directly reflecting transcriptional dynamics. As shown in Figure 1C, RNA velocity arrows indicate a trajectory from the melanoma subcluster of undifferentiated, neural crest (nc)-like cells on the left toward the more differentiated Mel_trans-melan_c7 and Mel_trans-melan_c8 subclusters at the right edge. LT analysis (Figure 1C) and the latent time heatmap (Figure 1D) revealed an opposing trajectory toward a more dedifferentiated state, exemplified by the Mel_trans subcluster. Here, melanoma cell dedifferentiation was linked to gene sets enriched in antigen presentation and the induction of T cell receptor signaling (Figure 1D). This aligns with the known association between high immune cell infiltrates and dedifferentiated tumors. Notably,

Abbreviations: ATAC, Assay for Transposase Accessible Chromatin; BACH1, BTB Domain And CNC Homolog; BLI, Bio-layer interferometry; CD2,3,28, cluster of differentiation 2,3,28; cDC1/2, type 1 and type 2 conventional dendritic cells; CRISPR, Clustered Regularly Interspaced Short Palindromic Repeats; Cas, CRISPR-associated protein; CAN, chromatin accessible networks; CREB1/5, CAMP Responsive Element Binding Protein 1/5; ETV5, ETS Variant Transcription Factor 5; Fb, fibroblasts; FN1, Fibronectin 1; FOSL2, FOS Like 2, AP-1 Transcription Factor Subunit; GEX, gene expression; gl, glands; GZMA, Granzyme A; HLA, human leukocyte antigen; IFNG, Interferon Gamma; IFN-γ, Interferon γ; ITGB1, Integrin Subunit Beta 1; JUN, Jun Proto-Oncogene, AP-1 Transcription Factor Subunit; JUNB, JunB Proto-Oncogene; KC, keratinocytes; premit, premitotic; postmit, postmitotic; LEF1, Lymphoid Enhancer Binding Factor 1; LT, latent time; Mel_trans_melan, melanoma transitory melanocytic cells; MHC, major histocompatibility complex; MITF, Melanocyte Inducing Transcription Factor; MM, primary malignant melanoma; Nev, benign melanocytic nevus/nevi; MYBL2, MYB Proto-Oncogene Like 2; NK, natural killer cells; PAX3, Paired Box 3; pDC, plasmacytoid dendritic cells; LE, lymphatic endothelial cells; RBPJ, Recombination Signal Binding Protein For Immunoglobulin Kappa J Region; RXRG, Retinoid X Receptor Gamma; scRNA-seq, single-cell RNA sequencing; SERPINE2, Serpin Family E Member 2; SOX2/4/10, SRY-Box Transcription Factor 2/4/10; TCF12, Transcription Factor 12; Tcyt, cytotoxic T cells; Tdp, double (CD4 and CD8) positive T cells; TEAD1, TEA Domain Transcription Factor 1; Teff_mem, effector memory T cells; Treg, regulatory T cells; TIL, tumor-infiltrating lymphocytes; UMAP, Uniform Manifold Approximation and Projection; TCGA, The Cancer Genome Atlas; VE, vascular endothelial cells; ZNF143, zinc finger protein 143.

[#]Antonia Stubenvoll and Maria Schmidt contributed equally to this work.

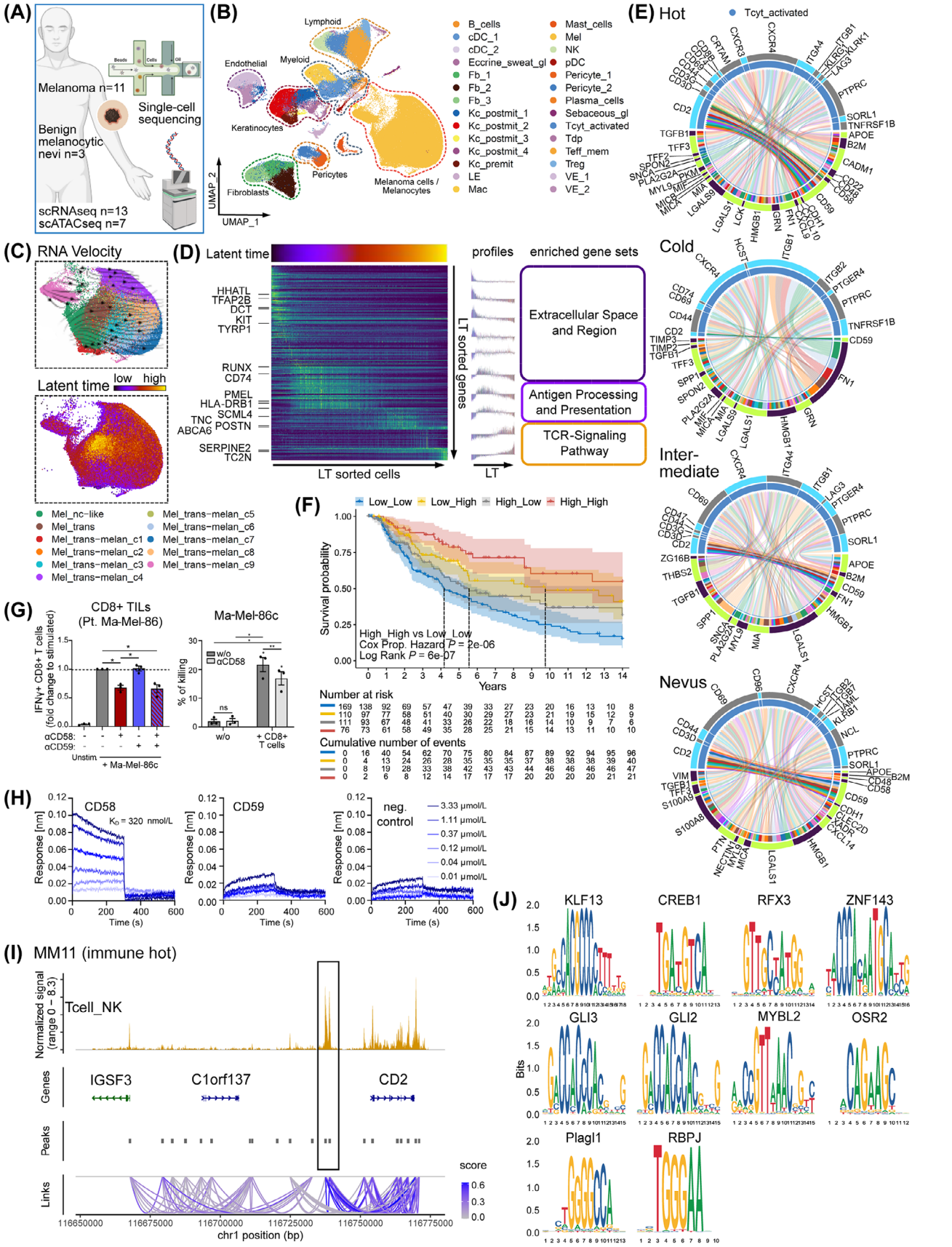

FIGURE 1 Single-cell RNA and single-cell ATAC sequencing of primary melanoma and melanocytic nevus samples. Ten primary melanoma samples (MM) and three benign melanocytic nevus (Nev) samples were analyzed by 10x Genomics single-cell RNA sequencing (scRNA-seq) technology. Five MM samples and one Nev sample were analyzed by single-cell ATAC (scATAC) sequencing. **(A)** Overview of

(Continues)

FIGURE 1 (Continued)
study design. **(B)** Analysis of scRNA-seq data from melanoma and nevus samples using the CellRanger software (10x Genomics), the R package Seurat (https://satijalab.org/seurat/) and principal component analysis (PCA). Specific cell type populations were identified by computing cell-type-specific positive markers using the FindAllMarkers function. Visualization was performed by Uniform Manifold Approximation and Projection (UMAP) of the integrated dataset, colored by cell type. **(C)** Zoom-in of the UMAP of the melanoma cell cluster from scRNA-seq data shown in (B). Gene expression data were analyzed by RNA velocity and latent time (LT) [4] analysis to show developmental trajectories of the melanoma cells. RNA velocity arrows point towards the right edge of the cluster, towards differentiated cells, and LT points in the opposite direction, towards de-differentiated cells, due to different mathematical approaches. **(D)** Heatmap of the dynamics of gene expression patterns during LT development of melanoma cells. LT profiles of 50 consecutive genes (top to bottom) reveal the shift of maximum gene expression from earlier to later LT. Examples of individual genes are highlighted, reflecting different stages of de-differentiation. Gene set enrichment is shown on the right. **(E)** scRNA-seq data from melanoma cells and cytotoxic T cells were subjected to ligand-receptor analysis using the LIANA software (https://saezlab.github.io/liana/). Circos plots of ligand-receptor interactions between different melanoma cell differentiation subtypes (lower part, in different colors) and T cells (upper part, in blue). The indicated genes of melanoma subclusters in the lower parts encompass different melanoma subclusters. The indicated genes of T cells in the upper parts encompass all receptors as arrowheads of different melanoma cell ligands. The figure legend for melanoma subclusters in panel (C) also applies to the inner rings of the circus plots in (E). **(F)** Melanoma patient survival data from The Cancer Genome Atlas (TCGA). Survival curves of melanoma patients with high and low levels, respectively, of CD58 and CD2 expression using patient data from TCGA. "High-high" indicates high CD58 and high CD2 expression; "low-low" indicates low CD58 and low CD2 expression. Analysis was performed using cSurvival (https://tau.cmmt.ubc.ca/cSurvival/). Significance levels were determined by a Cox proportional hazards model and Log-rank test. **(G)** Activation of autologous $CD8^+$ tumor-infiltrating lymphocytes (TILs) by melanoma cells in co-culture in the presence or absence of antibodies blocking CD58 and/or CD59. Left: Quantification of IFN-γ-producing $CD8^+$ T cells. Fold change is given as the mean±SEM from three independent experiments. The first column indicates IFN-γ-production in T cell monoculture. Right: Cytotoxicity of $CD8^+$ TIL against autologous Ma-Mel-86c cells in the presence or absence of an anti-CD58 blocking antibody. The percentage of killed melanoma cells is given as the mean±SEM from three independent experiments. Significantly different experimental groups are indicated: * $P < 0.05$, ** $P < 0.01$ by two-tailed paired *t*-test. **(H)** Recombinant proteins were generated for human CD2, CD58, and CD59. Bio-layer interferometry (BLI) measurements for recombinant CD2 protein interaction with recombinant CD58, CD59, and a negative control protein (SARS-CoV-2 receptor binding domain) were performed. Binding between these interaction partners was measured with CD58, CD59, and negative control concentrations ranging from 3.33 μmol/L to 0.01 μmol/L, with baseline at c = 0 μmol/L. The dissociation constant (Kd) for CD58 with CD2 was calculated as 0.99 (R^2 of concentration response curve). **(I)** Single-cell Assay for Transposase Accessible Chromatin sequencing (scATAC-seq) was performed on single-cell nuclei from melanoma cells of different samples and analyzed by CellRanger software (10x Genomics). Peak information was converted to genomic ranges using the GenomicRanges package (https://bioconductor.org/packages/release/bioc/html/GenomicRanges.html). A representative sample from 6 measured samples is shown, with signal tracks from the indicated genomic region. This figure refers to melanoma sample MM11 (immune hot). Signal tracks were generated using the RunChromVAR function in the Signac package (https://github.com/stuart-lab/signac). Co-accessible links were determined with the Cicero R package (https://github.com/cole-trapnell-lab/cicero-release). **(J)** The highlighted peak upstream of CD2 in melanoma samples was analyzed for binding motives of transcription factors. The analysis was conducted using the RunChromVAR function from the Signac package (https://github.com/stuart-lab/signac/issues/9), in combination with the JASPAR2020 motif databank, based on the BSgenome.Hsapiens.UCSC.hg38 genome (https://jaspar2020.genereg.net/tools/; https://www.ncbi.nlm.nih.gov/datasets/genome/GCF_000001405.40/). Binding motifs at the indicated genomic position are shown for different transcription factors in two representative melanoma samples (MM06; immune hot and MM09; immune intermediate).
Abbreviations: ATAC, Assay for Transposase Accessible Chromatin; Fb, fibroblasts; KC, keratinocytes; premit, premitotic; postmit, postmitotic; gl, glands; LE, lymphatic endothelial cells; VE, vascular endothelial cells; Tcyt, cytotoxic T cells; Tdp, double (CD4 and CD8) positive T cells; Teff_mem, effector memory T cells; Treg, regulatory T cells; NK, natural killer cells; cDC1/2, type 1 and type 2 conventional dendritic cells; pDC, plasmacytoid dendritic cells; LT, latent time; Pt., patient; Ma-Mel-86c, Mannheim melanoma cell line 86c; TCGA, The Cancer Genome Atlas; TIL, tumor-infiltrating lymphocytes; BLI, Bio-layer interferometry; SARS-CoV-2, severe acute respiratory syndrome coronavirus type 2.

Serpin Family E Member 2 *(SERPINE2)* has been identified as a mediator of melanoma metastasis and tumor progression [5].

Next, we performed regulon analysis (https://github.com/aertslab/pySCENIC) of the melanoma cell clusters, which refers to a group of genes regulated by the same transcription factor [6]. We identified a number of regulons associated with nc-like and more dedifferentiated melanoma cells, such as Retinoid X Receptor Gamma (*RXRG*), SRY-Box Transcription Factor 2 (*SOX2*), CAMP Responsive Element Binding Protein 5 (*CREB5*), BTB Domain And CNC Homolog (*BACH1*), and Transcription Factor 12 (*TCF12*), as well as those associated with more differentiated melanocytic cells, such as Melanocyte Inducing Transcription Factor (*MITF*), SOX10, Paired Box 3 (*PAX3*), TEA Domain Transcription Factor 1 (*TEAD1*),

and *SOX4* (Supplementary Figure S4). In line with this, it is known that BACH1 activates the expression of genes involved in cell motility and metastasis and plays an essential role in both innate and adaptive immune responses [7]. Taken together, melanoma cell dedifferentiation processes may be defined by an activated immune response and by specific transcriptional mechanisms.

Next, we focused on melanoma-immune cell interactions by analyzing ligand-receptor interactions with an emphasis on cytotoxic T cells, using the LIANA software (https://saezlab.github.io/liana/) (Figure 1E; Supplementary Tables S7 and S8). For a more focused analysis, we removed HLA and collagen genes from the subsequent analysis. As shown in Figure 1E, CD2 on cytotoxic T cells was a major interaction partner for several molecules in melanoma cells, especially CD58 and CD59. This interaction was most prominent in hot tumors. A recent study using a CRISPR/Cas knockout screen provided evidence that the CD58-CD2 interaction may indeed be a major mechanism of melanoma immune control [8]. Our data suggest that CD58 and CD59, both interacting with CD2, may control the T cell-melanoma cell interaction. In contrast, the most prominent interaction in cold tumors was between Fibronectin1 (FN1) and Integrin Subunit Beta 1 (ITGB1). Fibronectin-integrin β1 interaction is known to antagonize integrin β3 and thus might have an inactivating effect on integrin downstream signaling [9].

Immunofluorescence staining for CD58, CD59 and CD2 expression in melanoma/nevus samples (Supplementary Figure S5; Supplementary Table S9) showed higher numbers of $CD2^+$ immune cells in the vicinity of melanoma cells in hot/intermediate tumors compared to cold tumors/nevi. However, nevi do express both CD58 and CD2. Moreover, CD58 expression was higher in hot/intermediate samples and increased with increasing LT (Supplementary Figure S5).

Using data from The Cancer Genome Atlas (TCGA) melanoma cohort (https://www.genome.gov/Funded-Programs-Projects/Cancer-Genome-Atlas), we demonstrated that high CD58, together with high CD2 expression, significantly improved the prognosis of melanoma patients (Figure 1F, Supplementary Figure S6). Similarly, CD2 expression was associated with overall survival in a recently published melanoma immunotherapy study, making it a possible target for immunotherapy (Supplementary Figure S6).

Next, we used isolated tumor-infiltrating lymphocytes (TILs) enriched in tumor-reactive $CD8^+$ T cells from tumor tissue of a melanoma patient. As shown in Figure 1G and Supplementary Figure S7, T cell activation, as determined by intracellular Interferon γ (IFN-γ) expression, was reduced by blockade of CD58, but not of CD59, on autologous melanoma cells. Moreover, melanoma cell killing in the presence of T cells could be inhibited by the addition of the anti-CD58 antibody (Figure 1G).

Soluble recombinant extracellular domains of CD58, CD59 and CD2 were then used to measure the binding affinity of CD2 to CD58 and CD59, respectively (Figure 1H). These analyses showed high binding activity of CD2 to CD58, but none to CD59, which further supports an activating role of CD58-CD2, but not CD59-CD2. Overall, in addition to its known inactivating capacity on the membrane attack complex, CD59 appears to require a specific conformation to be active in the CD2 immune context, which may explain its inactivity in our settings.

Finally, scATAC-seq data of six MM and one Nev sample were analyzed in T cell populations (Figure 1I; Supplementary Tables S10 and S11). Among the top ten open chromatin regions in T cells from immune hot samples were *CD3D*, Interferon Gamma (*IFNG*), *CD28*, *CD2*, *CD3G*, and Granzyme A (*GZMA*). In line with this, *CD2* expression was most prominent in the T cell and NK cell clusters of the scATAC-seq UMAP and scRNA-seq UMAP (Supplementary Figure S8). By analyzing chromatin accessible networks (CAN), an open chromatin region was observed immediately upstream of the *CD2* gene (Figure 1I), which harbored a binding motif for various transcription factors, including *CAMP* Responsive Element Binding Protein 1 (*CREB1*), Zinc Finger Protein 143 (*ZNF143*), MYB Proto-Oncogene Like 2 (*MYBL2*), Recombination Signal Binding Protein For Immunoglobulin Kappa J Region (*RBPJ*), Jun Proto-Oncogene, AP-1 Transcription Factor Subunit (*JUN*), JunB Proto-Oncogene (*JUNB*), and FOS Like 2, AP-1 Transcription Factor Subunit (*FOSL2*) (Figure 1J, Supplementary Figure S8, Supplementary Figure S9). RBPJ might play an important role in this setting since it has been associated with T cell immune response in hepatocellular carcinoma and may thus be a target in immunotherapy [10].

Taken together, a detailed map of melanoma single-cell differentiation steps in MM and Nev lesions is presented, supporting a developmental trajectory of different melanoma cellular subpopulations towards a high immune phenotype. The CD58-CD2 interaction appears to play a prominent role in the melanoma immune response, which may be exploited in future clinical trials.

AUTHOR CONTRIBUTIONS

Antonia Stubenvoll: conceptualization, data curation, formal analysis, investigation, methodology, visualization, and writing original draft. Maria Schmidt: conceptualization, data curation, formal analysis, investigation, methodology, software, and writing original draft. Johanna Moeller: investigation, formal analysis, and methodology. Max Alexander Lingner Chango: data curation,

formal analysis, and investigation. Henry Loeffler-Wirth: investigation, methodology, data curation, formal analysis, validation, and visualization. Stephan Bernhart: investigation, methodology, data curation, formal analysis, validation and visualization. Florian Große: data curation, formal analysis, investigation, methodology, software and writing original draft. Carolyn Schultz: data curation, investigation, validation, and visualization. Olga Antoniadou: investigation, validation, and visualization. Beatrice Thier: investigation, formal analysis, investigation, and methodology. Annette Paschen: investigation, formal analysis, investigation, methodology, and supervision. Ulf Anderegg: investigation, formal analysis, investigation, methodology, and supervision. Jan C. Simon: resources, supervision, validation, writing, review, and editing. Mirjana. Ziemer: resources, investigation, writing, review, and editing. Clara T. Schoeder: data curation, conceptualization, investigation, validation, visualization, and supervision. Hans Binder: data curation, formal analysis, software, writing, review, and editing. Manfred Kunz: conceptualization, data curation, funding acquisition, investigation, project administration, resources, supervision, writing, review, and editing. All authors reviewed and approved the final version of the manuscript.

ACKNOWLEDGEMENTS

Not applicable

CONFLICT OF INTEREST STATEMENT

Manfred Kunz has received honoraria from the Speakers Bureau of Roche Pharma and travel support from Novartis Pharma GmbH and Bristol-Myers Squibb GmbH. Jan Christoph Simon has received speaker's fees from Bristol-Myers Squibb, Roche Pharma AG, Novartis and MSD Sharp & Dohme as well as financial support for congress attendance from Bristol-Myers Squibb, MSD Sharp & Dohme and Novartis. Mirjana Ziemer has received speaker's fees from Bristol-Myers Squibb, MSD Sharp & Dohme GmbH, Pfizer Pharma GmbH and Sanofi-Aventis Deutschland GmbH and received financial support for congress participation from Bristol-Myers Squibb and serves as a member of expert panels on cutaneous adverse reactions for Pfizer INC. Clara Tabea Schoeder has received research support from Navigo Protein GmbH, Halle (Saale), Germany.

FUNDING INFORMATION

This work was supported by the Deutsche Forschungsgemeinschaft (DFG) (German Research Foundation; grant numbers: KU 1320/10-1 and HO 6586/1-1, and SFB1430, project 424228829) and the Sächsische Aufbaubank (grant number: 10071450).

ETHICS APPROVAL AND CONSENT TO PARTICIPATE

Single-cell transcriptomic analyses were approved by the local Ethics committee of the Medical Faculty (AZ 023-16-01022016). Biopsies were taken after informed consent of the patients.

DATA AVAILABILITY STATEMENT

Sequencing data were uploaded to GEO data bank (https://www.ncbi.nlm.nih.gov/geo/), accession number: GSE277165. Other data will be provided upon reasonable request.

Antonia Stubenvoll[1,#]
Maria Schmidt[2,#]
Johanna Moeller[3]
Max Alexander Lingner Chango[3]
Carolyn Schultz[1]
Olga Antoniadou[1]
Henry Loeffler-Wirth[2]
Stephan Bernhart[4]
Florian Große[5,6]
Beatrice Thier[7]
Annette Paschen[7]
Ulf Anderegg[1]
Jan C. Simon[1]
Mirjana Ziemer[1]
Clara T. Schoeder[3]
Hans Binder[2]
Manfred Kunz[1]

[1]*Department of Dermatology, Venereology and Allergology, University of Leipzig Medical Center, Leipzig, Germany*
[2]*Interdisciplinary Center for Bioinformatics, University of Leipzig, Leipzig, Germany*
[3]*Institute for Drug Discovery, University of Leipzig Medical Center, Leipzig, Germany*
[4]*Bioinformatics Group, Department of Computer Science, University of Leipzig, Leipzig, Germany*
[5]*Department of Diagnostics, Fraunhofer Institute of Cell Therapy and Immunology (IZI), Leipzig, Germany*
[6]*Center for Scalable Data Analytics and Artificial Intelligence (ScaDS.AI) Dresden/Leipzig, Leipzig, Germany*
[7]*Department of Dermatology, University Hospital Essen, University Duisburg-Essen and German Cancer Consortium (DKTK), Partner Site Essen/Düsseldorf, Essen, Germany*

Correspondence
Manfred Kunz; Department of Dermatology, Venereology and Allergology, University of Leipzig Medical Center, Leipzig 04103, Germany.
Email: manfred.kunz@medizin.uni-leipzig.de

Hans Binder; Interdisciplinary Center for Bioinformatics, University of Leipzig, Leipzig 04107, Germany.
Email: binder@izbi.uni-leipzig.de

ORCID

Manfred Kunz https://orcid.org/0000-0002-5950-5586

REFERENCES

1. Boutros A, Croce E, Ferrari M, Gili R, Massaro G, Marconcini R, et al. The treatment of advanced melanoma: Current approaches and new challenges. Crit Rev Oncol Hematol. 2024;196:104276.
2. Reynolds G, Vegh P, Fletcher J, Poyner EFM, Stephenson E, Goh I, et al. Developmental cell programs are co-opted in inflammatory skin disease. Science 2021;371(6527):eaba6500.
3. Tsoi J, Robert L, Paraiso K, Galvan C, Sheu KM, Lay J, et al. Multi-stage Differentiation Defines Melanoma Subtypes with Differential Vulnerability to Drug-Induced Iron-Dependent Oxidative Stress. Cancer Cell. 2018;33:890–904.e5.
4. Bergen V, Lange M, Peidli S, Wolf FA, Theis FJ. Generalizing RNA velocity to transient cell states through dynamical modeling. Nat Biotechnol. 2020;38:1408–1414.
5. Wu QW. Serpine2, a potential novel target for combating melanoma metastasis. Am J Transl Res. 2016;8:1985–1997.
6. Jiang T, Zhou W, Chang Z, Zou H, Bai J, Sun Q, et al. ImmReg: the regulon atlas of immune-related pathways across cancer types. Nucleic Acids Res. 2021;49:12106–12118.
7. Igarashi K, Nishizawa H, Saiki Y, Matsumoto M. The transcription factor BACH1 at the crossroads of cancer biology: From epithelial-mesenchymal transition to ferroptosis. J Biol Chem. 2021;297:101032.
8. Frangieh CJ, Melms JC, Thakore PI, Geiger-Schuller KR, Ho P, Luoma AM, et al. Multimodal pooled Perturb-CITE-seq screens in patient models define mechanisms of cancer immune evasion. Nat Genet. 2021;53:332–341.
9. Su C, Mo J, Dong S, Liao Z, Zhang B, Zhu P. Integrinβ-1 in disorders and cancers: molecular mechanisms and therapeutic targets. Cell Commun Signal. 2024;22:71.
10. Pan B, Wang Z, Zhang X, Shen S, Ke X, Qiu J, et al. Targeted inhibition of RBPJ transcription complex alleviates the exhaustion of CD8+ T cells in hepatocellular carcinoma. Commun Biol. 2023;6:123.

SUPPORTING INFORMATION

Additional supporting information can be found online in the Supporting Information section at the end of this article.